**ESKİŞEHİR TEKNİK ÜNİVERSİTESİ BİLİM VE TEKNOLOJİ DERGİSİ**
**B- TEORİK BİLİMLER**

Eskişehir Technical University Journal of Science and Technology B- Theoretical Sciences

**Estuscience – Theory, 2025, 13 (2) pp. 77-91, DOI:10.20290/estubtdb.1566835**

**RESEARCH ARTICLE**

# BIOLOGICAL ACTIVITIES WITH IN SILICO STUDY OF BTDE COMPOUND AS INHIBITORS OF MYCOBACTERIUM TUBERCULOSIS PROTEIN-TARGETS, ADME AND DFT CALCULATIONS

**Ahmet Çağrı ATA[1, *], Ümit YILDIKO [2]**

[1] Department of Chemistry, Faculty of Arts and Sciences Faculty, Kafkas University, Kars, Turkey
ahmetata1024@gmail.com - 0000-0002-2296-2265

[2] Department of Bioengineering, Architecture and Engineering Faculty, Kafkas University, Kars, Turkey
yildiko1@gmail.com - 0000-0001-8627-9038

**Abstract**

Tuberculosis caused by Mycobacterium is currently treated with chemotherapeutic antibiotics. A new molecule, β-hydroxytriazole, was evaluated as a Mycobacterium Tuberculosis inhibitor. Our strategy was to evaluate this compound for its optimized properties against Mycobacterium Tuberculosis. In this study, with 6-311++G(d,p) base set under the B3LYP/B3PW91 techniques, the target molecule 1-(1-benzyl-1H-1,2,3-triazol-4-yl)-2-(2,4-dichlorophenyl) ethane-1,2-dione (BTDE) was optimized and its energy parameters were analyzed using density functional calculation (DFT). In addition to the optimized structure of the molecule, many quantum chemical parameters; HOMO-LUMO, MEP, Intramolecular electronic interactions and mullikene atomic charges were calculated and the obtained data were visualized. HOMO-LUMO analysis revealed that the molecule has NLO properties to a significant extent, with energy ranges close to each other in the basis sets used (-7.304/-7.368 eV) and (-1.349/-1.277 eV). The molecular docking analysis and pharmacological potential of BTDE compound were evaluated against the KasA enzymes of Mycobacterium tuberculosis. The results indicated that the compound exhibited strong binding affinities, with docking scores of -6.798 and -6.788 kcal/mol for the respective receptors. These findings suggest that the compound may serve as a promising inhibitor of these critical enzymes, highlighting its potential in tuberculosis treatment.

**Keywords**

Tuberculosis,
DFT,
KasA enzyme,
Molecular docking

**Time Scale of Article**

Received :14 October 2024
Accepted : 17 March 2025
Online date : 25 August 2025

## 1. INTRODUCTION

Tuberculosis (TB) is a highly contagious disease caused by the bacterium Mycobacterium tuberculosis [1]. It primarily affects the lungs (pulmonary tuberculosis) but can also impact other organs such as the kidneys, spine, and brain (extrapulmonary tuberculosis) [2, 3]. The disease is spread through the air when an infected individual expels bacteria by coughing, sneezing, or even speaking, making it particularly contagious in crowded or poorly ventilated environments. Certain populations, including individuals with compromised immune systems—such as those with diabetes, HIV/AIDS, or malnutrition —are more susceptible to contracting TB [4]. Multidrug-resistant tuberculosis (MDR-TB) has become a public health problem that does not respond to typical first-line treatments [5]. Global efforts, including vaccination with Bacillus Calmette-Guérin (BCG) and sustained treatment with antibiotics, are essential in combating the spread of this life-threatening disease [6]. However, delayed

*Corresponding Author: ahmetata1024@gmail.com

diagnosis, inadequate healthcare infrastructure, and poor adherence to treatment regimens contribute to the persistence of TB in many parts of the world [7].

The strategy for synthesizing the desired β-hydroxytriazoles, which serve as key precursors for α,β-ketotriazoles and styryl derivatives, involves a multi-step approach that ensures both selectivity and efficiency [8]. For β-hydroxytriazoles, a subsequent nucleophilic addition of an appropriate carbonyl compound, such as an aldehyde or ketone, to the triazole core is carried out. This step is often catalyzed by a base or an acid, depending on the reaction conditions, to facilitate the formation of the desired β-hydroxy group. The stereoselectivity of this addition can be controlled by choosing the right catalysts and reaction conditions, depending on the desired configuration. The β-hydroxytriazoles obtained through this method can then be oxidized to yield α,β-ketotriazoles, an important class of intermediates in various chemical transformations [9]. Oxidizing agents such as Dess-Martin periodinane (DMP) or PCC (pyridinium chlorochromate) are typically employed to selectively oxidize the hydroxyl group without affecting the triazole ring [10].

For the synthesis of styryl derivatives, further functionalization of the β-hydroxytriazoles or α,β-ketotriazoles can be achieved by condensation with styryl precursors, such as aldehydes or halides, through coupling reactions [10]. These derivatives are significant due to their applications in pharmaceuticals and materials science. The choice of reagents and catalysts in these final steps often depends on the nature of the desired styryl derivative, as well as the need for controlling the regio- and stereochemistry of the final product.Overall, this synthetic strategy provides a flexible and efficient route to access β-hydroxytriazoles, which are valuable intermediates for constructing more complex triazole-based compounds, such as α,β-ketotriazoles and styryl derivatives [11].

In this study, the specific structural and biological behaviors of the molecule were emphasized considering the pharmacological importance of BTDE. Chemical descriptors of the molecule, optimized parameters, NLO, MEP were obtained by DFT method with 6–311++G (d,p) basis set using the same level technique. In many different studies, the electrical properties of the conjugated π system in BTDE compound HOMO and LUMO energies were theoretically calculated to investigate. The inhibitory properties of the ligand on the Mycobacterium tuberculosis KasA enzyme were confirmed through molecular docking studies.

## 2. PREPARATION OF MANUSCRIPT

### 2.1. Theoretical Calculations

Here, the structural, electronic and chemical properties of the molecule were by DFT calculations using Gaussian 09 program [12]. HOMO-LUMO, molecular electrostatic potential (MEP), and chemical descriptor analyses were conducted using the same theoretical framework. The Gaussian View 06 software was utilized to visualize the three-dimensional structures and calculate parameters such as atomic charge distribution and electronic density, thereby enhancing our understanding of the electronic properties of the compounds. Molecular docking was performed to elucidate the binding mechanism of the ligand at the active site of the protein. The studies utilized Maestro version 11.8 [13] as the computational platform. Molecular docking is a computational technique widely used in drug discovery to predict how small molecules, such as drug candidates, bind to a receptor of known 3D structure. The main goal of molecular docking is to model the interaction between the ligand (the small molecule) and the target protein in order to identify the optimal orientation, conformation, and position of the ligand within the binding site of the protein. High-resolution crystal structures of Mycobacterium tuberculosis KasA enzymes (PDB ID: 6P9L and PDB ID: 6P9M) were retrieved from the RCSB Protein Data Bank (http://www.rcsb.org/pdb). The ligand structure of the synthesized compound was prepared following established protocols using the Ligprep module [14]. Docking studies were conducted using the Glide docking module, allowing for the calculation of optimal binding energies and poses between the ligand

and the protein. The resulting docking interactions were visualized with Discovery Studio version 4.5, providing insights into the ligand-protein interactions [15].

## 2.2. DFT Studies

### 2.2.1. Geometry optimization

Geometry optimization is employed to ascertain the most stable conformation of a molecule, specifically the configuration corresponding to the minimum energy state [16]. This process involves optimizing a multivariable function that incorporates parameters such as bond lengths, bond angles, and dihedral angles. By identifying these optimal geometric parameters, researchers can gain insights into the molecule's stability and reactivity, which are critical for understanding its chemical behavior and potential applications [17].

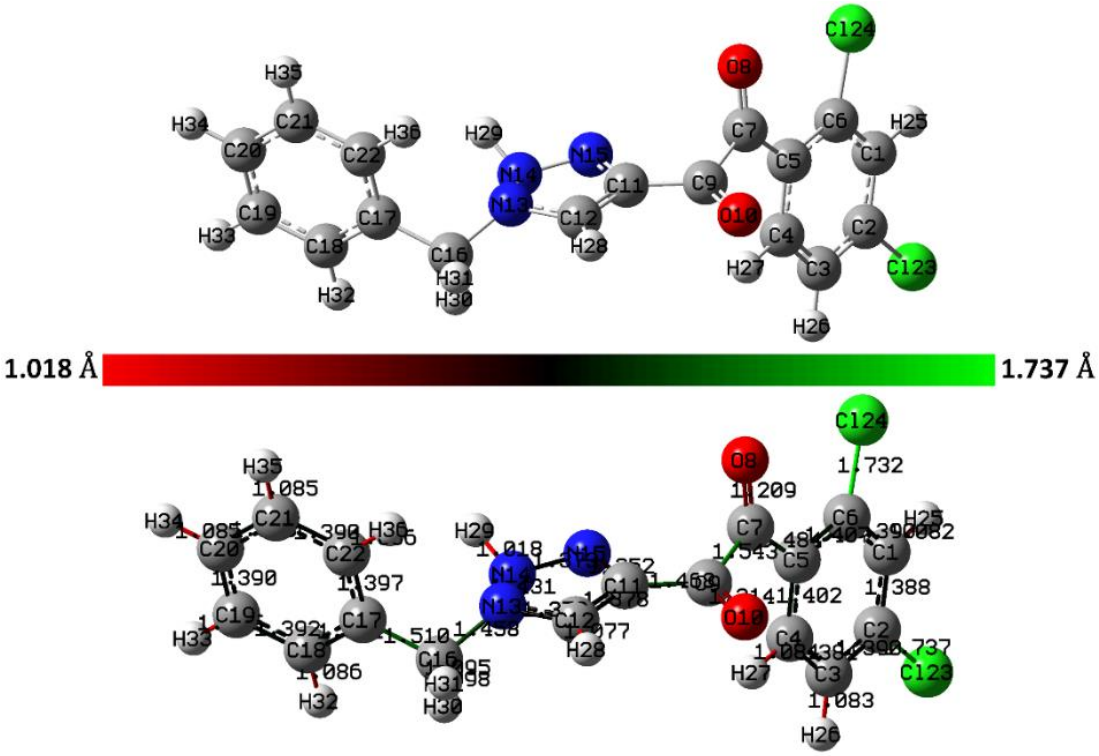


**Figure 1.** Optimized structure for BTDE using 6-311++G (d, p) basis sets with the DFT - B3LYP / B3PW91 methods.

As a result of the optimization, stable structures are found from the energy function calculated for the molecule and the coordinates corresponding to these structures are determined. Thus, to initiate quantum calculations, it is essential to determine the initial coordinates of the molecule [18]. This process is crucial for identifying the most stable conformation of the BTDE molecule. The optimized geometric structure and the corresponding total energy conversion are presented in Figure 1, illustrating the findings of the optimization process.

**Table 1.** Theoretically Obtained Geometric Parameters for BTDE

| Bond Lengths (Å) | | | Bond Angles (°) | | |
|---|---|---|---|---|---|
| **Atom Groups** | **B3LYP** | **B3PW91** | **Atom Groups** | **B3LYP** | **B3PW91** |
| C1-C2 | 1.389 | 1.399 | C1-C2-C3 | 121.31 | 119.99 |
| C1-H25 | 1.081 | 1.070 | C1-C2-Cl23 | 119.05 | 120.00 |
| C2-C3 | 1.391 | 1.402 | C9-C11-C12 | 126.34 | 125.28 |
| C2-Cl23 | 1.750 | 1.760 | C1-C6-Cl24 | 116.18 | 120.21 |
| C3-H26 | 1.081 | 1.069 | C2-C3-C4 | 118.36 | 120.43 |
| C4-C5 | 1.404 | 1.403 | C2-C3-H26 | 120.58 | 119.78 |
| C4-H27 | 1.082 | 1.069 | C2-C1-H25 | 120.61 | 120.22 |
| C6-Cl24 | 1.745 | 1.760 | C3-C4-H27 | 118.45 | 119.78 |
| C7-O8 | 1.210 | 1.258 | C5-C6-Cl24 | 122.83 | 120.22 |
| C7-C9 | 1.547 | 1.540 | C5-C7-O8 | 125.99 | 120.00 |
| C9-O10 | 1.216 | 1.258 | C7-C9-O10 | 119.18 | 119.99 |
| C9-C11 | 1.471 | 1.539 | C7-C9-C11 | 117.22 | 120.00 |
| C11-C12 | 1.379 | 1.343 | O8-C7-C9 | 115.36 | 120.00 |
| C11-N15 | 1.355 | 1.342 | C11-C12-N13 | 107.43 | 108.04 |
| C12-N13 | 1.376 | 1.325 | C11-C12-H28 | 130.18 | 125.96 |
| C12-H28 | 1.076 | 1.069 | C11-N15-N14 | 104.91 | 107.69 |
| N13-N14 | 1.442 | 1.404 | C12-N13-C16 | 123.60 | 125.12 |
| N13-C16 | 1.467 | 1.469 | N13-N14-N15 | 109.07 | 102.60 |
| N14-N15 | 1.381 | 1.414 | N13-C16-H31 | 106.03 | 109.47 |
| N14-H29 | 1.018 | 0.999 | N14-N13-C16 | 115.69 | 125.13 |
| C16-C17 | 1.514 | 1.539 | C17-C18-C19 | 120.57 | 119.99 |
| C16-H30 | 1.096 | 1.069 | C19-C18-H32 | 119.80 | 120.00 |
| C18-H32 | 1.085 | 1.069 | C19-C20-H34 | 120.15 | 119.99 |
| **Dihedral Angles (°)** | | | | | |
| **Atom Groups** | **B3LYP** | **B3PW91** | **Atom Groups** | **B3LYP** | **B3PW91** |
| C1-C2-C3-C4 | 0.07343 | -0.00635 | C4-C5-C7-O8 | -173.89879 | 179.96609 |
| C2-C1-C6-C5 | 0.12515 | -0.00422 | O8-C7-C9-O10 | -101.34075 | 179.92520 |
| C1-C2-C3-H26 | -179.78643 | 179.99377 | C7-C9-C11-C12 | -167.38253 | 179.70589 |
| C2-C1-C6-Cl24 | 179.55045 | 179.99194 | C11-N15-N14-N13 | 12.44977 | -15.21978 |
| C4-C3-C2-Cl23 | 179.96872 | 179.99237 | N14-N13-C16-H30 | 55.71355 | 89.77162 |
| Cl24-C6-C1-H25 | -0.40001 | -0.00939 | N13-C16-C17-C18 | 125.66363 | 149.97779 |
| H26-C3-C4-H27 | 0.33384 | -0.00802 | C17-C18-C19-C20 | 0.33196 | -0.01208 |
| O10-C9-C11-N15 | -172.71498 | -179.67266 | H33-C19-C20-H34 | 0.19079 | -0.00446 |
| C11-C12-N13-N14 | 10.22500 | -9.29979 | C11-N15-N14-H29 | 136.17523 | 103.06151 |

The optimized bond length parameters of the BTDE molecule, calculated using the 6-311++G (d, p) basis sets with DFT - B3LYP / B3PW91, are presented in Table 1. A comparison of the optimized methods indicates that the molecular structure corresponds to the minimum potential energy configuration. All bond lengths, bond angles, and dihedral angles within the phenyl rings fall within normal ranges. Specifically, the C-C bond distances are observed to be 1.389–1.513 Å for B3LYP and 1.343–1.539 Å for B3PW91, while the C-O bond distances, associated with the oxygen atom bridging the two phenyl rings, are measured at 1.210 Å and 1.258 Å. The C-H and C-Cl bond lengths in the aromatic ring range from 1.081 to 1.096 Å and from 1.750 to 1.760 Å, respectively. Additionally, the C-C-C angles range from 119° to 121°. Other bond angles in the compound include: C-C-H (118°–120°), C-C-O (115°–125°), C-C-N (107°–108°), N-N-N (109°), N-C-H (106°–109°), and O-C-H (109°–111°). The differences between the values obtained from the B3LYP and B3PW91 methods are minimal [19]. The theoretically calculated parameters for the BTDE compound provide valuable insights into the geometric changes of the molecule.

### 2.2.2. Molecular orbital theory

DFT calculation methods provide valuable insights into the structural properties of molecules. The energy and positioning of the HOMO-LUMO orbitals are particularly crucial for understanding electron exchange reactions, as they characterize charge transfer capabilities between electron-donating and

electron-accepting species [20]. Frontier molecular orbital (FMO) theory is instrumental in calculating various parameters, including optical and electronic properties, quantum chemistry, molecular reactivity, and both pharmaceutical and biological activities. The energy difference between the HOMO and LUMO orbitals indicates the stability and strength of the molecule [21]. FMOs also assist in identifying the most reactive regions of the compound. The theoretical energy values for the HOMO ($E_{HOMO}$) and LUMO ($E_{LUMO}$) orbitals, based on the employed basis sets, were calculated as -7.304 / -7.368 eV and -1.349 / -1.277 eV, respectively. The energy gap between the FMOs was found to be 6.091 / 5.955 eV, suggesting the bioactive potential of the molecule, as illustrated in Figure 2. Figure 2 further reveals that the vacant LUMO orbital is primarily situated on the aromatic benzene rings of the triazole compound, while the HOMO orbital, exhibiting π-character, is predominantly located on the nitrogen group, with minor contributions from the oxygen group [22]. The global chemical reactivity of the molecule is summarized in Table 2.

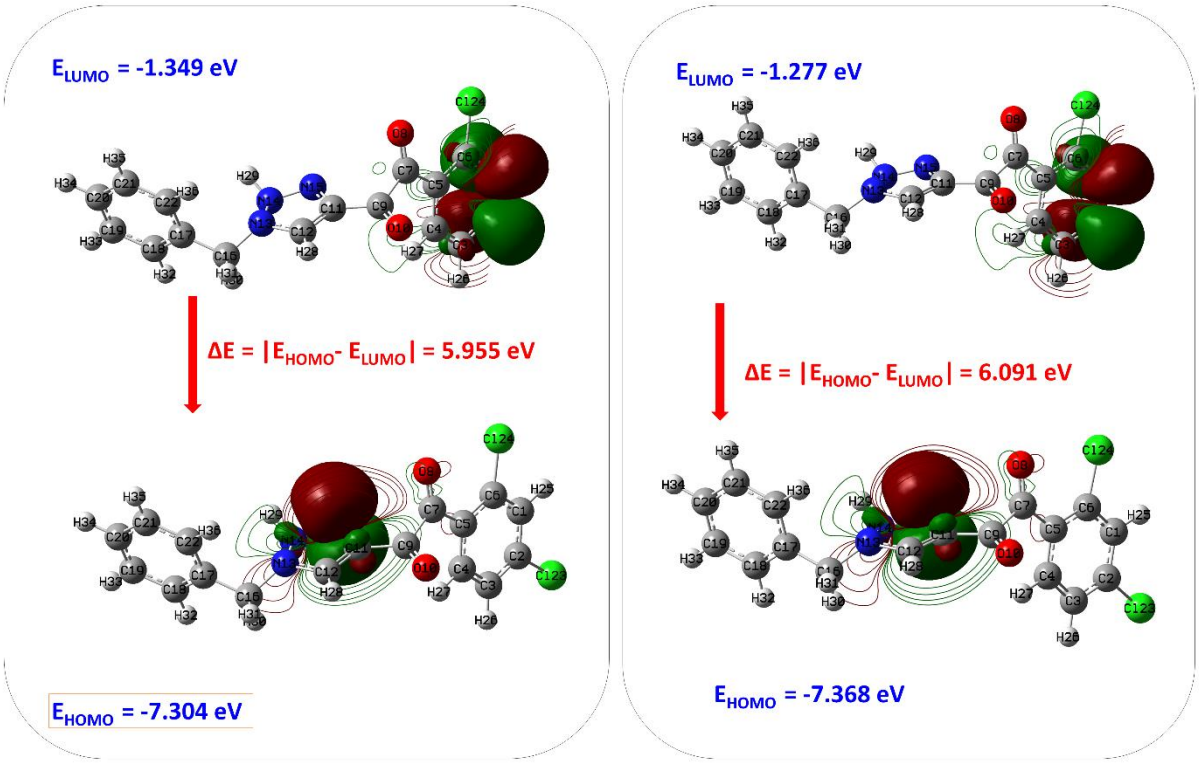


**Figure 2.** Energy levels of the BTDE molecule of FMO.

**Table 2.** Energy parameters* for the BTDE molecule's low energy conformers (in eV).

| | $E_{HOMO}$ | $E_{LUMO}$ | ΔE | I | A | η | s | μ | χ | ω |
|---|---|---|---|---|---|---|---|---|---|---|
| **B3LYP** | -7.304 | -1.349 | 5.955 | 7.304 | 1.349 | 2.978 | 1.489 | -4.327 | 4.327 | 3.144 |
| **B3PW91** | -7.368 | -1.277 | 6.091 | 7.368 | 1.277 | 3.046 | 1.523 | -4.323 | 4.323 | 3.068 |

ΔE→Energy Gaps, I→Ionization potential ($-E_{HOMO}$), A→Electron Affinity ($-E_{LUMO}$), η→Chemical Hardness, s→Global Softness, μ→Chemical Potential, χ→Electronegativity, ω→Global Electrophilicity.

The nonlinear optical (NLO) effect arises from the interactions of electromagnetic fields within various media, resulting in fields that are modified in terms of phase, frequency, and amplitude [23]. For the BTDE molecule, the calculated parameters are as follows: Dipole moment (μ) = 6.5642-6-5734 D, polarizability (α) = -145.5390 and -143.5066 au and first hyperpolarizability (β) = $7.5 \times 10^{-31}$ - 1.7 x10$^{-}$

$^{31}$ esu (Table 3). These parameters highlight the potential of the molecule for applications in NLO materials, indicating its responsiveness to external electromagnetic fields [24].

**Table 3.** Calculated NLO Parameters for BTDE

| Parameter | B3LYP | B3PW91 | Parameter | B3LYP | B3PW91 |
|---|---|---|---|---|---|
| $\mu_x$ | -5.4829 | -5.4816 | $\beta_{XXX}$ | 107.3729 | -103.2597 |
| $\mu_y$ | -3.6032 | -3.6258 | $\beta_{XXY}$ | 10.1076 | 4.1762 |
| $\mu_z$ | 0.2073 | 0.1256 | $\beta_{XYY}$ | -25.9708 | -26.8590 |
| $\mu_{(D)}$ | 6.5642 | 6.5734 | $\beta_{YYY}$ | -18.5307 | -19.3842 |
| $\alpha_{xx}$ | -126.2737 | -124.1181 | $\beta_{XXZ}$ | -57.9836 | -62.0294 |
| $\alpha_{yy}$ | -155.5312 | -153.1338 | $\beta_{XYZ}$ | -13.5850 | -11.2818 |
| $\alpha_{zz}$ | -154.8123 | -153.2681 | $\beta_{YYZ}$ | 1.2423 | 1.0846 |
| $\alpha_{XY}$ | -3.7111 | -3.2534 | $\beta_{XZZ}$ | -19.8141 | -20.7903 |
| $\alpha_{XZ}$ | 0.0752 | -0.1194 | $\beta_{YZZ}$ | -6.9082 | -5.9658 |
| $\alpha_{YZ}$ | -3.4089 | -4.0210 | $\beta_{ZZZ}$ | 16.5550 | -15.3797 |
| α (au) | -145.5390 | -143.5066 | β (esu) | 7.5 x $10^{-31}$ | 1.7 x$10^{-31}$ |

### 2.2.3. Mulliken atomic charges

The electronic charge densities play a critical role in the application of quantum chemical calculations to molecular systems. These quantities influence various properties, including dipole moment, polarizability, and chemical reactivity, all of which depend on charge distribution within the molecular framework [25]. The Mulliken atomic charges, calculated using the DFT - B3LYP / B3PW91 methods with 6-311++G (d, p) basis sets, are illustrated in Figure 3. This representation provides insights into the electronic characteristics of the molecule and aids in understanding its behavior in different chemical environments.

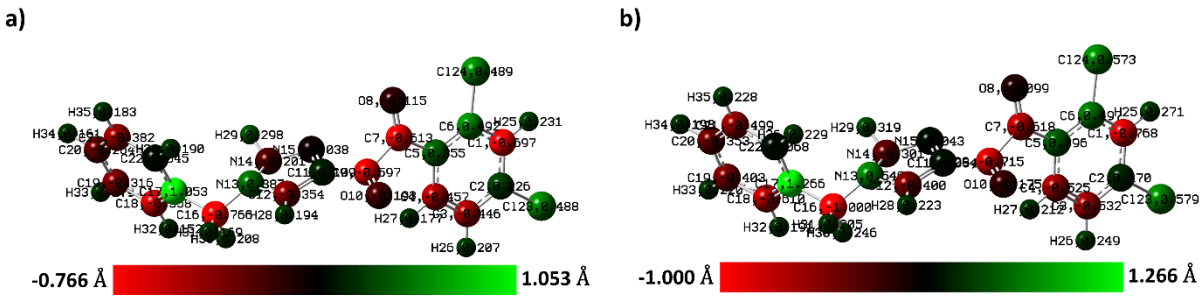


**Figure 3.** Mulliken atomic charges of the molecule

From Table 4, it can be observed that the charges on the carbon atoms (C7, C9, C11, C12) are higher than those of the other carbon atoms in the compound. This phenomenon occurs because these carbon atoms are bonded to electronegative oxygen atoms (O8, O10) and nitrogen atoms (N13, N14, N15). Furthermore, the nitrogen and oxygen atoms (O8, O10, N13, N14, and N15) exhibit the most negative charges, indicating that these centers possess the highest electron density [26]. As a result, they are likely to engage in favorable interactions with the positively charged regions of potential receptors, enhancing the molecule's reactivity and binding capabilities [27].

**Table 4.** Mulliken atomic charges (in a.u.) at important atomic sites of the molecule.

| Atoms | B3LYP | B3PW91 | Atoms | B3LYP | B3PW91 | Atoms | B3LYP | B3PW91 |
|---|---|---|---|---|---|---|---|---|
| C1 | -0.696 | -0.767 | N13 | 0.387 | 0.549 | H25 | 0.231 | 0.271 |
| C2 | 0.226 | 0.169 | N14 | -0.201 | -0.300 | H26 | 0.207 | 0.248 |
| C3 | -0.445 | -0.531 | N15 | -0.037 | 0.042 | H27 | 0.176 | 0.212 |
| C4 | -0.456 | -0.524 | C16 | -0.765 | -0.999 | H28 | 0.194 | 0.223 |
| C5 | 0.355 | 0.396 | C17 | 1.053 | 1.265 | H29 | 0.298 | 0.318 |
| C6 | 0.491 | 0.497 | C18 | -0.558 | -0.610 | H30 | 0.208 | 0.245 |
| C7 | -0.612 | -0.617 | C19 | -0.316 | -0.403 | H31 | 0.168 | 0.204 |
| O8 | -0.114 | -0.099 | C20 | -0.264 | -0.352 | H32 | 0.152 | 0.190 |
| C9 | -0.596 | -0.715 | C21 | -0.382 | -0.499 | H33 | 0.178 | 0.220 |
| O10 | -0.193 | -0.174 | C22 | 0.045 | 0.067 | H34 | 0.161 | 0.198 |
| C11 | 0.109 | 0.064 | Cl23 | 0.488 | 0.579 | H35 | 0.183 | 0.227 |
| C12 | -0.353 | -0.400 | Cl24 | 0.488 | 0.573 | H36 | 0.190 | 0.229 |

### 2.2.4. Molecular electrostatic potential surfaces

MEPS provide a three-dimensional representation of the charge distribution within molecules, which is crucial for analyzing intramolecular interactions and assessing the reactivity of hydrogen bonds towards electrophilic or nucleophilic attacks [25]. The most active sites for such attacks in the BTDE molecule were calculated using the DFT method with the 6-311++G (d,p) basis set, and the MEPS surface is illustrated in Figure 4. In this representation, red, blue, and green colors denote regions of varying electrostatic potential. Specifically, the red region indicates areas around the oxygen atom that are prone to electrophilic interactions, while the nitrogen atom also exhibits electrophilic reactivity. Conversely, the blue regions, associated with hydrogen atoms, signify sites that are more reactive towards nucleophilic attacks. This visualization effectively highlights the potential reactivity of the molecule, guiding further exploration of its chemical behavior.

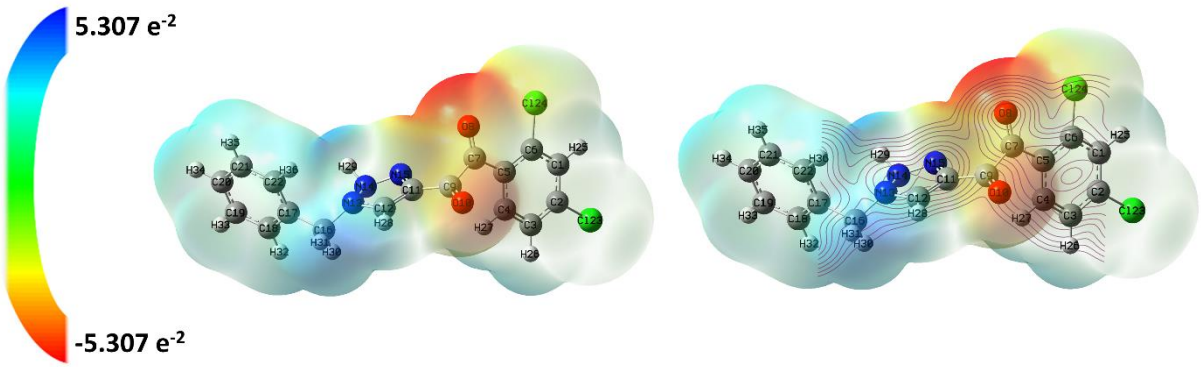


**Figure 4.** Molecular electrostatic potential maps of BTDE

### 2.2.5. Molecular docking

Pharmacological data and drug design studies play a crucial role in understanding the biochemical performance of potential therapeutic compounds. These investigations focus on analyzing how drugs interact with biological targets, primarily proteins, to elucidate their efficacy, mechanism of action, and

therapeutic potential [28]. One of the most important aspects of this research is categorizing protein-ligand interactions, which refers to the binding of a drug (ligand) to its specific protein target, such as enzymes or receptors, which is central to the drug's biological activity. To accurately predict and analyze these interactions, the molecular docking method is widely employed. Molecular docking is a computational technique used to model the interaction between a ligand and its target protein at the molecular level. It simulates the potential binding modes of the ligand in the protein's active site, estimating both the strength and specificity of the interaction. The goal is to predict the optimal conformation of the ligand that leads to the most favorable interaction, which directly correlates with the drug's potential effectiveness.

By integrating pharmacological data, such as binding affinity and inhibitory constants, with molecular docking results, researchers can better understand the thermodynamics and kinetics of these interactions. This information helps in refining drug design by identifying key molecular features that contribute to strong protein-ligand binding. Furthermore, it aids in the identification of potential off-target effects or adverse interactions, ultimately supporting the development of more selective and effective therapeutic agents. Thus, the combination of pharmacological data, protein-ligand interaction studies, and molecular docking methods forms a powerful framework for rational drug design, enabling the development of new drugs with improved efficacy and minimized side effects.

In this study, the in silico enzyme inhibition activity of the synthesized ligands was experimentally confirmed. The development of inhibitors targeting Mycobacterium tuberculosis KasA, a key enzyme in the fatty acid synthesis pathway of Mycobacterium tuberculosis (Mtb), has been an area of significant interest for anti-tuberculosis drug discovery [29]. KasA plays a critical role in the elongation of fatty acids that are essential for the biosynthesis of mycolic acids, which are crucial components of the Mtb cell wall and contribute to its virulence and resistance to host defenses [30]. To confirm the mode of inhibition of the synthesized compound at the molecular level, interactions between the enzyme and the protein receptor molecules were analyzed through molecular docking, with results presented in Figure 5. Inhibitors targeting Mycobacterium tuberculosis are frequently employed to alleviate the symptoms of tuberculosis. The calculated binding energy of -6.798 kcal/mol indicates a strong affinity of the synthesized compound for the Mycobacterium tuberculosis KasA protein structure, suggesting effective binding and potential for therapeutic application. This interaction underscores the compound's promise in combating tuberculosis [31]. The bonds of van der Waals bond to the Mycobacterium tuberculosis KasA active site of the molecule; . LEU 205, GLY 200 HIS 345, SER 346, GLU 120, GLU 203, PHE 210 can be given. There are also ALA 119 5.43 Å PHE 239 5.25 Å π-π satcked, PRO 206 5.99 Å LEU 116 5.53 Å ILE 347 5.48 Å π-alkyl interactions. Because of its capacity to form hydrogen bonds, this extremely active substance is also believed to be capable of significant inhibition of enzyme activity. [32]. The docking results highlight the specific binding modes, where the compound forms stabilizing interactions, such as hydrogen bonds, hydrophobic contacts, or van der Waals forces, with the active site of the protein. These interactions help to confirm the compound's potential to inhibit the protein's function, thereby suggesting its relevance as a bioactive molecule in therapeutic applications. Furthermore, the docking analysis provides insights into the affinity and specificity of the binding, which are important parameters for assessing the compound's efficacy as a drug candidate.

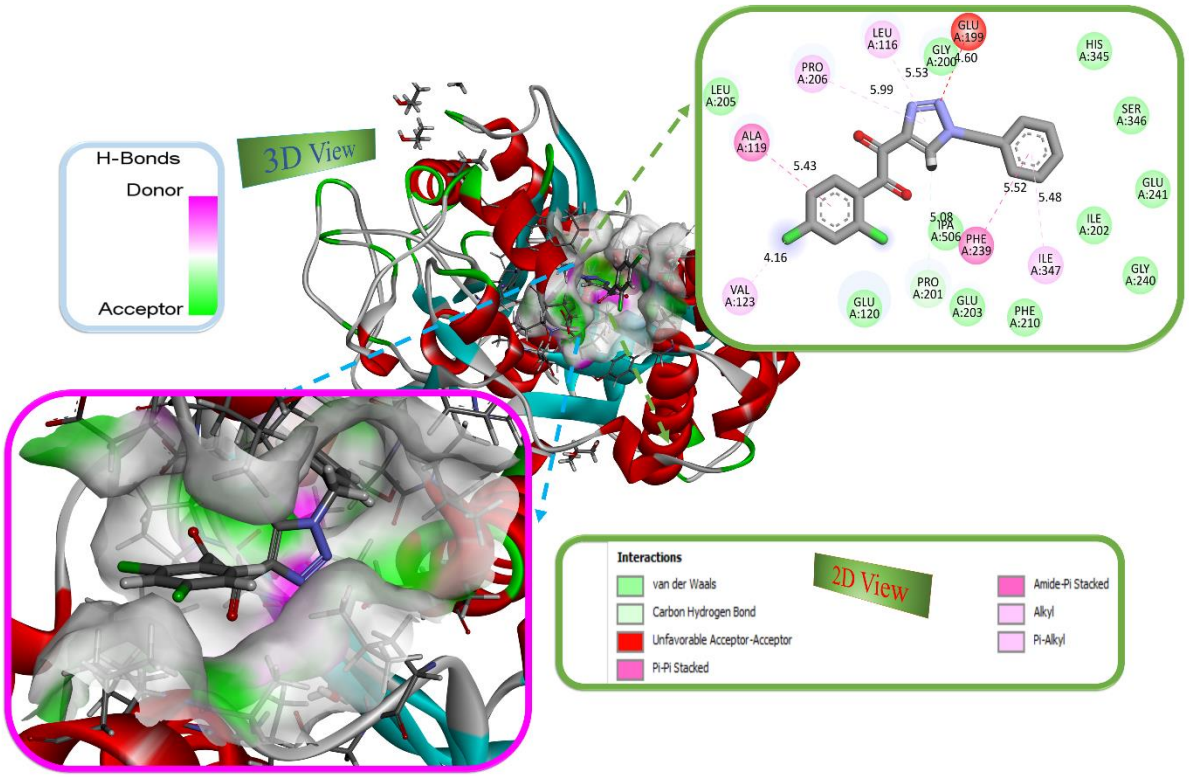


**Figure 5.** 3D View of Ligand-Protein Interactions: Hydrogen Bond Donor/Acceptor Surface

The compound binds to the catalytic active site of the enzyme with a total binding energy of -6.788 kcal/mol, achieved through intermolecular interactions. This docking analysis focused on the most favorable binding mode, which is illustrated in Figure 6. The results indicate that the compound exhibits a strong binding affinity towards the acetylcholinesterase (AChE) enzyme, suggesting its potential as an effective inhibitor. This favorable interaction highlights the compound's suitability for further development in therapeutic applications targeting AChE. GLY 240 PHE 210 GLU 203 LEU 205 LEU 116 SER 346 HIS345 van der Waals, IPA 507 3.95 Å and 3.28 Å hydrogen bond, PRO 201 4.67 3.37 conventional hydrogen bonds, ILE 202 4.87 Å alkyl, PHE 239 4.49 PRO 206 5.51 ALA 119 5.71 π-alkyl GLU 241 3.75 halogen bonds THE 239 4.14 π-π satcked GLY 200 4.15 Amid π satcked. Molecular docking studies further substantiated the inhibitory activities of the compounds, providing valuable insights into the interactions between the ligands and enzyme active sites [33]. These analyses highlighted critical binding interactions, including hydrogen bonds, hydrophobic interactions, and electrostatic forces, which collectively contribute to the stabilization of the ligand within the enzyme's active site. Understanding these interactions is essential for optimizing ligand design and enhancing the efficacy of potential inhibitors in therapeutic applications [34]. The docking analysis also helped to elucidate the binding conformation and orientation of the compounds, which are critical for their inhibitory efficacy.

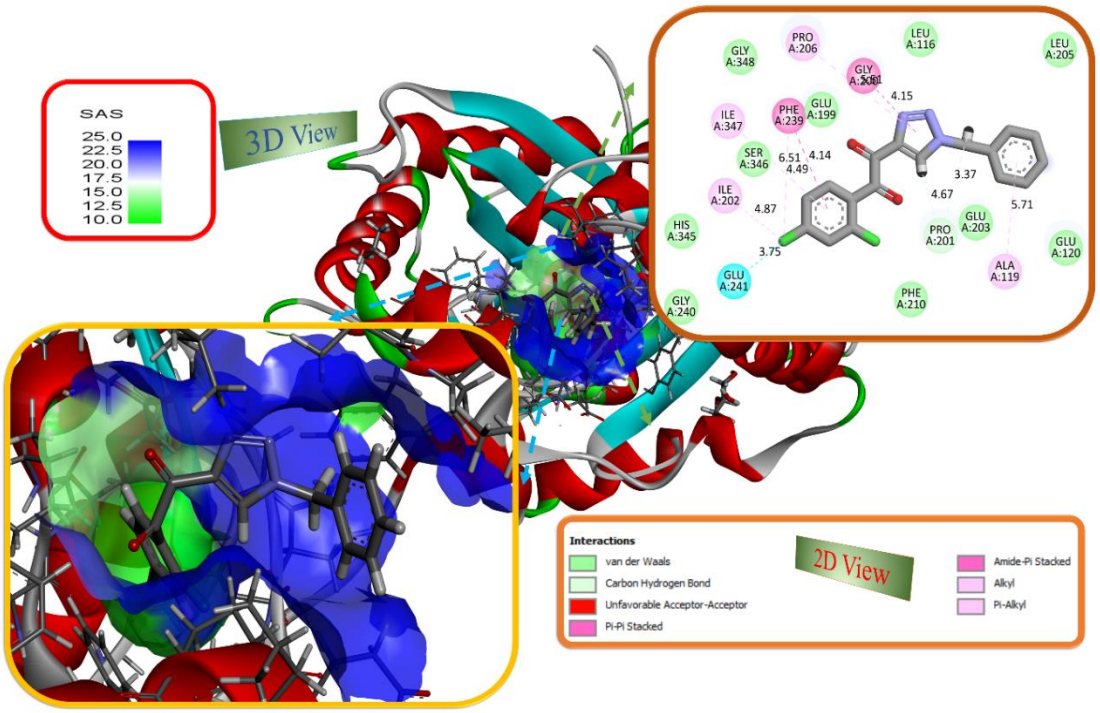


**Figure 6.** Mode of interaction with Ligand-Protein enzymes; 3D view of solvent interactions

### 2.2.7. Pharmacokinetic analysis

These assessments provide essential insights into the compound's behavior within biological systems, helping to predict its efficacy, safety, and potential therapeutic application. Understanding ADME characteristics is vital for optimizing the compound's design and ensuring that it reaches its target effectively while minimizing adverse effects [35]. Proper ADME profiling ensures that the compound not only exhibits biological activity but also possesses the necessary characteristics to be effective as a drug candidate. In clinical trials, it is essential that the ADME properties of a candidate drug are balanced to ensure sufficient bioavailability, optimal distribution to target tissues, efficient metabolism, and appropriate excretion rates.

To evaluate the drug-like efficacy of the phthalonitrile compound designed in this study, Lipinski's Rule of Five was applied. This set of guidelines helps predict the oral bioavailability of a compound, stating that a potential drug is more likely to be successful if it satisfies the following criteria: (1) no more than 5 hydrogen bond donors, (2) no more than 10 hydrogen bond acceptors, (3) a molecular weight under 500 Daltons, and (4) a logP (octanol-water partition coefficient) less than 5, indicating appropriate lipophilicity [36]. Bioavailability is the percentage of a state or active device that passes through the systemic passage. The permeability of the membrane is the ability of a molecule to cross the cell membrane. The LogP value of 3.732 indicates moderate lipophilicity, suggesting the molecule has a good balance between hydrophilic and hydrophobic properties. This should allow effective membrane permeability and decent bioavailability, as molecules with LogP values between 1 and 4 typically show good absorption and distribution. However, further studies are needed to confirm its impact on solubility and overall bioavailability in a biological setting. As a result, the LogP value plays an important summary role in the healing process of the two interactions.

The application of Lipinski's rules to the phthalonitrile compound confirmed its potential as a viable drug candidate, suggesting it is likely to possess favorable pharmacokinetic properties, such as good

absorption and membrane permeability. However, further studies, including in vivo ADME testing and optimization, are needed to fully assess its clinical potential. Table 5 shows the values obtained. The colored zone in Figure 7 indicates the physicochemical area suitable for oral bioavailability, highlighting optimal ranges for key properties that enhance absorption and distribution.

**Table 5.** The ADME 2.0 online analysis parameters in the evaluation of the BTDE compound

| | | | |
|---|---|---|---|
| Molecular Weight | 359.02 | f-Char | 0 |
| Density | 1.083 | n-Rig | 19 |
| n-HA | 5 | Flexibility | 0.263 |
| n-HD | 0 | Stereo-Centers | 0 |
| n-Rot | 5 | TPSA | 64.85 |
| nRing | 3 | Log-S | -5.287 |
| Max-Ring | 6 | Log-P | 3.732 |
| n-Het | 7 | Log-D | 3.325 |

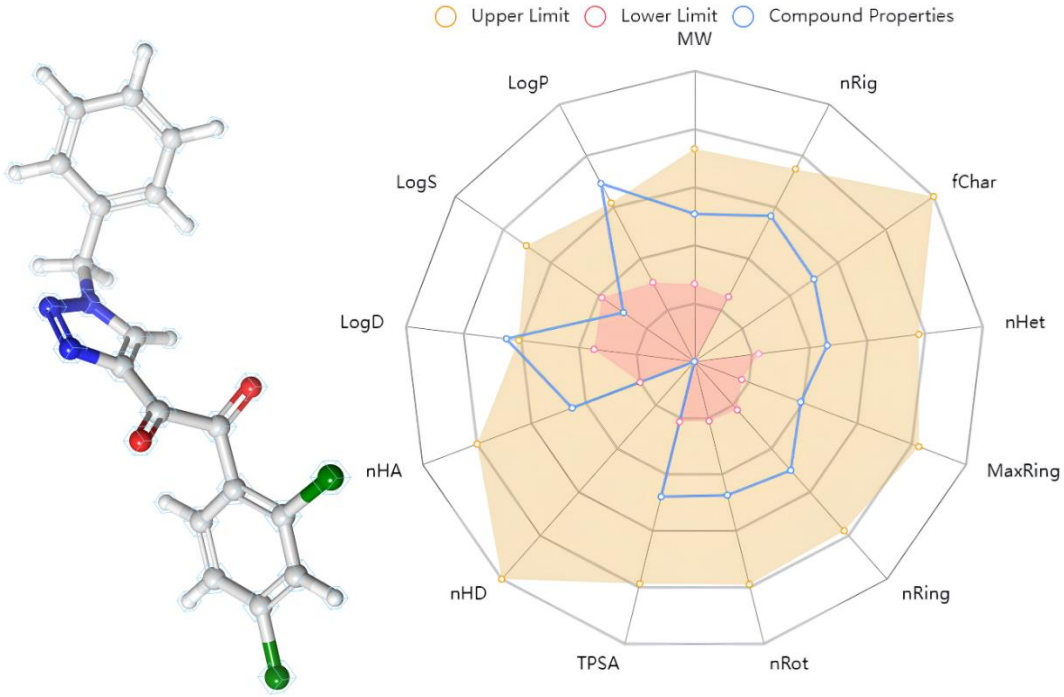


**Figure 7.** Color regions and pharmacological parameters of the compound.

## 3. CONCLUSIONS

The geometric optimization (bond length, bond angle and dihedral angle etc.), HOMO-LUMO analysis and spectroscopic structure of BTDE molecule were carried out using with 6-311++G(d,p) base set under the B3LYP/B3PW91 methods. The same method was used to calculate the optimized geometric parameters. In addition, due to its high hyperpolarizability, BTDE molecule has strong NLO activity and the results are in better agreement with each other. The molecule exhibits a binding affinity of -6.798 and -6.788 kcal/mol, indicating a strong interaction. The molecular electrostatic potential map reveals that the hydrogen atoms are surrounded by positive potential regions, while the oxygen atoms are located in more electronegative areas. This analysis also highlights the energy gap of the investigated molecule and the chemical stability of its reactive regions. Furthermore, the ligand's docking

performance and interactions with Mycobacterium tuberculosis KasA enzyme receptors correlate well with the inhibition studies. Overall, in silico analyses suggest that this compound is a promising candidate for drug design processes.

## CONFLICT OF INTEREST

The authors stated that there are no conflicts of interest regarding the publication of this article.

## CRediT AUTHOR STATEMENT

**Ahmet Çağrı Ata:** Formal analysis, Writing - original draft, Official analysis, Verification, Visualization, Conceptualization. **Ümit Yıldıko:** Methodology, Software, Validation, Investigation, Writing – Review & Editing, Supervision.

## REFERENCES

[1] Gunawan G, Koraag M, Syahnuddin M, Nursafingi A, Nurjana M, Sumolang P, Murni, Hidayah N & Irawati. Strain identification of mycobacterium tuberculosis in multidrug-resistant tuberculosis (mdr-tb) patients at undata hospital, palu, Central Sulawesi. IJTB 2023; 71

[2] Karanis G & Karanis P, Tuberculosis: Epidemiology and global impact, including extrapulmonary tuberculosis manifestation with emphasis on skeletal tuberculosis and a rare example of shoulder tuberculosis from tibetan plateau Area, 2019.

[3] Pascual-Pareja JF, Carrillo-Gómez R, Hontañón-Antoñana V & Martínez-Prieto M. Treatment of pulmonary and extrapulmonary tuberculosis. Enferm Infecc Microbiol Clin (Engl Ed) 2018; 36 (8):507-516.

[4] Giri S, Sahu P, Kanungo S, Bal HB, Kumar S, Kar S, Mohanty T, Turuk J, Das D & Hota PK. Diabetes mellitus and human immunodeficiency virus (HIV) infection in people with tuberculosis in Odisha, India. IJTB 2024; 71 (2):147-152.

[5] Mphaphuli MT, Sithole MN, Kumar P, Kondiah PP, Mabrouk M & Choonara Y E. Multi-purpose prototypes for extrapulmonary Mycobacterium tuberculosis targeting: A regenerative medicine perspective. J Drug Deliv Sc 2023; 89:105039.

[6] Guo F, Wei J, Song Y, Song J, Wang Y, Li K, Li B, Qian Z, Wang X & Wang H. Immune responses induced by Mycobacterium tuberculosis heat-resistant antigen (Mtb-HAg) upon co-administration with Bacillus Calmette-Guérin in mice. Cytokine 2024; 179:156610.

[7] Olowoyo KS, Esan DT, Adeyanju BT, Olawade DB, Oyinloye BE & Olowoyo P. Telemedicine as a tool to prevent multi-drug resistant tuberculosis in poor resource settings: Lessons from Nigeria. JCTUBE 2024:100423.

[8] Aguirre-Pranzoni C, Tosso RD, Bisogno FR, Kurina-Sanz M & Orden AA. Preparation of chiral β-hydroxytriazoles in one-pot chemoenzymatic bioprocesses catalyzed by Rhodotorula mucilaginosa. Process Biochem 2019; 79:114-117.

[9] Menendez C, Rodriguez F, Ribeiro A L d J L, Zara F, Frongia C, Lobjois V, Saffon N, Pasca M R, Lherbet C & Baltas M. Synthesis and evaluation of α-ketotriazoles and α, β-diketotriazoles as inhibitors of Mycobacterium tuberculosis. Eur J Med Chem 2013; 69:167-173.

[10] Kaspar M & Kudova E. Selectivity of oxidizing agents toward axial and equatorial hydroxyl groups. J Org Chem 2022; 87 (14):9157-9170.

[11] Giraudo A, Krall J, Nielsen B, Sørensen T E, Kongstad K T, Rolando B, Boschi D, Frølund B & Lolli M L. 4-Hydroxy-1, 2, 3-triazole moiety as bioisostere of the carboxylic acid function: a novel scaffold to probe the orthosteric γ-aminobutyric acid receptor binding site. Eur J Med Chem 2018; 158:311-321.

[12] Frisch M. gaussian 09, Revision d. 01, Gaussian. Wallingford CT 2009; 201

[13] Bursal E, Yılmaz MA, Aras A, Türkan F, Yildiko Ü, Kılıç Ö & Dey A. Determination of phenolic content, biological activity, and enzyme inhibitory properties with molecular docking studies of Rumex nepalensis, an endemic medicinal plant. JFNR 2021; 9 (3):114-123.

[14] Alshehri B, Vijayakumar R, Senthilkumar S, Ismail A, Abdelhadi A, Choudhary RK, Albenasy KS, Banawas S, Alaidarous MA & Manikandan P. Molecular target prediction and docking of anti-thrombosis compounds and its activation on tissue-plasminogen activator to treat stroke. J King Saud Univ Sci 2022; 34 (1):101732.

[15] Biovia D S, Discovery studio modeling environment, Release San Diego, CA, 2017.

[16] Lee J, Lee K, Noh M & Lee S H. Optimal density functional theory to predict electron affinities of polycyclic aromatic hydrocarbon molecules. Chem Phys Lett 2024; 856:141646.

[17] El-Asri A, Jmiai A, Bourzi H, Lin Y & El Issami S. Chemistry of the interaction between Imidazole derivatives as corrosion inhibitors molecules and copper/brass/zinc surfaces: A DFT, reactive and classical molecular force fields study. Surf Interfaces 2024; 44:103799.

[18] Ahmed ZK, Ermiş T & Ermiş E. Theoretical and experimental study on (E)-N'-(2-hydroxy-5-(thiophen-3-yl) benzylidene) benzohydrazide compound: Its optimization with DFT and Fuzzy logic approach (FLA), structural and spectroscopic investigation, HOMO-LUMO, MEP, atomic charge, and NBO analysis. J Mol Struct 2024; 1315:138829.

[19] Yildiko Ü, Türkan F, Tanriverdi AA, Ata AC, Atalar MN & Cakmak I. Synthesis, enzymes inhibitory properties and characterization of 2-(bis (4-aminophenyl) methyl) butan-1-ol compound: Quantum simulations, and in-silico molecular docking studies. J Indian Chem Soc 2021; 98 (11):100206.

[20] Türker L & Azizoğlu A. The Effect of boron substitution on cyclacenes. J Mol Struct THEOCHEM 2001; 535 (1-3):151-157.

[21] Tekeş AT, Ata AÇ, Tanrıverdi AA & Çakmak İ. Insilico molecular docking studies of THBF compound: TD-DFT simulations and drug design. JIST 2021; 11 (4):2955-2966.

[22] Sani MJ. Theoretical survey on the electronic, linear and nonlinear optical properties of substituted benzenes and polycondensed π-systems. A density functional theory study. Comput Theor Chem 2023; 1223:114100.

[23] Nadeem S, Anwar A, Khan MU, Hassan AU & Alrashidi KA. Exploring the ON/OFF nonlinear optical (NLO) response in tetracene-based chromophores: A DFT study on solvent and frequency-dependent NLO properties for switching applications. J Mol Liq 2024; 411:125730.

[24] Aiman U, Adeel M, Haroon M, Ahmed A, Hussain A, Rehman MAU, Bullo S & Alhokbany N. Highly efficient donor-acceptor configurated Nicotinaldehyde-based small molecules for NLO materials: Base-free deformylation and DFT study. J Mol Struct 2024; 1310:138195.

[25] Solgun DG, Tanriverdi AA, Yildiko U & Ağirtaş MS. Synthesis of axially silicon phthalocyanine substituted with bis-(3, 4-dimethoxyphenethoxy) groups, DFT and molecular docking studies. J Incl Phenom Macrocycl Chem 2022; 102 (11):851-860.

[26] Gören K, Bağlan M & Yıldıko Ü. Melanoma cancer evaluation with ADME and molecular docking analysis, DFT calculations of (E)-methyl 3-(1-(4-methoxybenzyl)-2, 3-dioxoindolin-5-yl)-acrylate molecule. JIST 2024; 14 (3):1186-1199.

[27] Samson Y, Dhas D A & Joe IH. Exploration of Non Covalent Interactions, Structural, Vibrational, Chemical Reactivity and NLO Properties of 1, 2-Diphenyl-2-Methoxyethanone Oxime: A Theoretical Approach. PACs 2023; 43 (8)

[28] Kalaimathi K, Thiyagarajan G, Vijayakumar S, Bhavani K, Karthikeyan K, Rani JMJ, Dass K, Sureshkumar J & Prabhu S. Molecular docking and network pharmacology-based approaches to explore the potential of terpenoids for Mycobacterium tuberculosis. Pharmacol Res Mod Chin Med 2021; 1:100002.

[29] Jayaraman M, Rajendra SK & Ramadas K. Structural insight into conformational dynamics of non-active site mutations in KasA: A Mycobacterium tuberculosis target protein. Gene 2019; 720:144082.

[30] Franklin MC, Rudolph MJ, Ginter C, Cassidy MS & Cheung J. Structures of paraoxon‐inhibited human acetylcholinesterase reveal perturbations of the acyl loop and the dimer interface. Proteins Struct. Funct. Bioinf 2016; 84 (9):1246-1256.

[31] Schiebel J, Kapilashrami K, Fekete A, Bommineni GR, Schaefer CM, Mueller MJ, Tonge PJ, & Kisker C. Structural basis for the recognition of mycolic acid precursors by KasA, a condensing enzyme and drug target from Mycobacterium tuberculosis. JBC 2013; 288 (47):34190-34204.

[32] Khan IM, Khan A, Shakya S & Islam M. Exploring the photocatalytic activity of synthesized hydrogen bonded charge transfer co-crystal of chloranilic acid with 2-ethylimidazole: DFT, molecular docking and spectrophotometric studies in different solvents. J Mol Struct 2023; 1277:134862.

[33] Scarpi-Luttenauer M, Galentino K, Orvain C, Cecchini M, Gaiddon C & Mobian P. $TiO_4N_2$ complexes formed with 1, 10-phenanthroline ligands containing a donor-acceptor hydrogen bond site: Synthesis, cytotoxicity and docking experiments. Inorganica Chim Acta 2022; 540:121036.

[34] Gören K & Yıldıko Ü. Aldose reductase evaluation against diabetic complications using ADME and molecular docking studies and DFT calculations of spiroindoline derivative molecule. Süleyman Demirel univ fen bilim enst derg 2024; 28 (2):281-292.

[35] Anbu V, Karthick T & Vijayalakshmi K. Combined experimental and computational approach for the vibrational characteristics and theoretical evaluation of binding activities and ADME Descriptors of 2, 6-Di-Tert-Butyl-p-Cresol. PACs 2022; 42 (4):1169-1185.

[36] Chagas CM, Moss S & Alisaraie L. Drug metabolites and their effects on the development of adverse reactions: revisiting Lipinski's rule of five. Int J Pharm 2018; 549 (1-2):133-149.